Seventh International Conference on
Computational Fluid Dynamics (ICCFD7),
Big Island, Hawaii, July 9-13, 2012

ICCFD7-2902

Direct numerical simulation of compressible multi-phase flow with a pressure-based method

M. Boger*, F. Jaegle*, S. Fechter*, B. Weigand** and C.-D. Munz*
Corresponding author: markus.boger@iag.uni-stuttgart.de

* Institute of Aerodynamics and Gas Dynamics, University of Stuttgart, Germany.
** Institute of Aerospace Thermodynamics, University of Stuttgart, Germany.

Abstract: In this contribution we present a pressure-based numerical scheme for the direct numerical simulation of two-phase flows. While for many technical applications, two-phase flows can be treated as incompressible, this assumption fails in cases with high pressure and temperature as they can be found in rocket combustion chambers, for example. Our interest is in the development of a pressure-based method that aims at the extension of an incompressible two-phase code to the compressible regime. The development builds upon a method that has originally been designed for single-phase flows. Its adaptation to three-dimensional (3D) two-phase flows is shown. This includes the possibility to resolve and track the interface as well as the description of the two phases by different equations of state. Furthermore, it is shown that the scheme does not necessitate a cumbersome interface treatment in three dimensions in order to avoid spurious oscillations in the vicinity of the material interface. To improve the interface tracking, we present the coupling of the pressure-based flow solver to a discontinuous Galerkin approach for the level set transport equation and we show first results. Numerical examples of shock-droplet interactions indicate the capability of the approach to simulate excellently the propagation of shock waves in gaseous and liquid phases, including multiple wave reflections.

Keywords: Compressible multi-phase flow, DNS, pressure-based method, level set.

1 Introduction

Direct numerical simulation (DNS) of two-phase flows including the resolution of the material interface is usually performed with the incompressible Navier-Stokes equations. Typical technical applications concern droplets in an air environment at ambient pressure. In such a configuration, the liquid itself can be considered to be almost incompressible. Usually, the droplets are moving at low speed, such that the compressibility of the gas can also be neglected. Under these circumstances, kinetic and internal energy are decoupled resulting in the separation of thermodynamics and hydrodynamics. This separation comes along with different roles of pressure for compressible and incompressible flows. The incompressible pressure is decoupled from density and internal energy, as an equation of state (EOS) is not present. Therefore, pressure is of purely hydrodynamic nature and loses its thermodynamic meaning.

In the context of fuel injection processes, more extreme ambient conditions have to be faced that are characterized by an augmented pressure and temperature. Especially for large pressure and temperature gradients in the flow field, the thermodynamic effects can no longer be neglected and have to be taken into account by the numerical simulation in order to get accurate results. This requires the compressible flow equations.

The simulation of multiphase flows is always characterized by large jumps in the material properties across the interface separating two phases. An additional difficulty is the resolution and tracking of the interface itself. Both issues are of great importance for incompressible and compressible flows. However, the use of the compressible flow equations introduces different EOS on either side of the material interface. As the

fluids can differ significantly in their properties, their EOS are also very different in nature. Problems may arise due to the numerical smearing of the density across the material interface that represents a contact discontinuity. When inserted into the EOS, the smeared density causes an unphysical pressure. From a mathematical point of view, this represents a stiff problem and the change in EOS is very challenging as it results quite often in spurious pressure and velocity oscillations in the vicinity of the interface, if there is no special remedy applied [1].

Our interest lies in the extension of an incompressible two-phase flow solver to the compressible regime. Numerically, the incompressible flow equations are solved by the so-called pressure-based schemes while the simulation of compressible flows is usually performed with density-based methods. Yet, there are several possibilities to extend an originally incompressible pressure-based method to the compressible flow equations. One of these approaches builds upon an asymptotic pressure decomposition, introducing multiple pressure variables. The compressible pressure is split into a hydrodynamic pressure and a thermodynamic background pressure. While the thermodynamic pressure is spatially constant and only depending on time, the hydrodynamic pressure is allowed to vary in space and time. The decomposition considers the different roles of pressure for compressible and incompressible flows and allows the transition from the fully compressible flow equations to their incompressible limit case. This scheme is called the Multiple Pressure Variables (MPV) method [2]. Its conservative formulation [3] is the basis of the numerical scheme that is described in this paper. The MPV method has been derived for single-phase flows [2, 3] and extended to the treatment of compressible two-phase flows in one space dimension [4]. In this paper we now present its extension to three space dimensions including its validation with the simulation of 3D shock-droplet interactions. Moreover, first steps have been undertaken to enhance the interface resolution. An improved evaluation of the surface normals and curvature is important for surface tension and other interfacial phenomena. We describe the coupling of a spectral element discontinuous Galerkin (DG) approach [5, 6] for the high-order interface tracking to the pressure-based flow solver and discuss first results.

The outline of the paper is as follows. In the next section, the governing equations are presented. Afterwards the MPV method and its extension to the treatment of 3D multiphase flows are described. It is shown how the compressible pressure-based flow solver treats the interface including the coupling of a high-order DG level set method for the interface tracking. This is followed by the presentation and discussion of the simulation of two shock-droplet interactions. First results are presented for the coupling of the level set DG approach to the pressure-based finite volume flow solver before the paper closes with a short conclusion and a perspective on future work.

2 Governing equations

This section gives an overview over the equations that build the basis of our numerical scheme.

2.1 Compressible Euler equations

We use the 3D conservation equations for mass, momentum and total energy for inviscid flows without gravitational and external forces and heat conduction in compressible gas dynamics that are known as the Euler equations

$$\frac{\partial \rho'}{\partial t'} + \nabla \cdot (\rho' \mathbf{v}') = 0\,, \tag{1}$$

$$\frac{\partial (\rho' \mathbf{v}')}{\partial t'} + \nabla \cdot [(\rho' \mathbf{v}') \circ \mathbf{v}'] + \nabla p' = 0\,, \tag{2}$$

$$\frac{\partial e'}{\partial t'} + \nabla \cdot [\mathbf{v}' (e' + p')] = 0\,. \tag{3}$$

Here, ρ' denotes the density, p' the pressure, $\mathbf{v}'$ the velocity and e' the total energy per unit volume. Dimensional variables are marked by the superscript $'$. The system (1)-(3) has to be closed with an EOS relating the pressure to the known flow variables. A well-known formulation for gaseous fluids is the perfect

gas EOS

$$p' = (\gamma - 1)(e' - \frac{\rho'}{2}|\mathbf{v}'|^2), \tag{4}$$

with γ being the adiabatic exponent. For liquids like water, the Tait EOS is used

$$p' = (\gamma - 1)(e' - \frac{\rho'}{2}|\mathbf{v}'|^2) - \gamma(k_0 - p_0). \tag{5}$$

Here, p_0 and k_0 are constants where the latter determines the compressibility of the fluid. However, there also exists the so-called stiffened gas EOS [7] that combines both previous EOS and that is used in the following

$$p = (\gamma - 1)(e' - \frac{\rho'}{2}|\mathbf{v}'|^2) - \gamma p_\infty. \tag{6}$$

The constant p_∞ characterizes the compressibility of the fluid. It is obvious that (6) includes the ideal gas EOS (4) by choosing $p_\infty = 0$ as well as the Tait fluid EOS (5) for $p_\infty = (k_0 - p_0)$.

The numerical scheme is based on the Euler equations in a dimensionless form and the following set of non-dimensional variables is introduced:

$$x = \frac{x'}{x_{ref}}, \quad \rho = \frac{\rho'}{\rho_{ref}}, \quad v = \frac{\mathbf{v}'}{|\mathbf{v}_{ref}|}, \quad p = \frac{p'}{p_{ref}}, \quad t = \frac{t'|\mathbf{v}_{ref}|}{x_{ref}}, \tag{7}$$

where the subscript *ref* denotes the reference values.

The pressure-based numerical method uses an asymptotic expansion of the pressure, such that the limit case of an incompressible flow is accessible. The speed of sound and the fluid velocity are given different reference values. This leads us to the introduction of a parameter called global flow Mach number M

$$M = \frac{|\mathbf{v}_{ref}|}{\sqrt{p_{ref}/\rho_{ref}}}, \tag{8}$$

that determines the compressibility of the flow. Using this set of variables the Euler equations (1)-(3) can be non-dimensionalized in the following way

$$\frac{\partial \rho}{\partial t} + \nabla \cdot (\rho \mathbf{v}) = 0, \tag{9}$$

$$\frac{\partial (\rho \mathbf{v})}{\partial t} + \nabla \cdot [(\rho \mathbf{v}) \circ \mathbf{v}] + \frac{1}{M^2}\nabla p = 0, \tag{10}$$

$$\frac{\partial e}{\partial t} + \nabla \cdot [(e + M^2 p)\mathbf{v}] = 0. \tag{11}$$

2.2 Level set method for the interface tracking

For the DNS of two-phase flows, the interface location is of crucial interest. Therefore, an additional transport equation is introduced to describe the movement of the material interface between the two fluids. Based on [8], a level set variable Φ is initialized as a signed distance function with respect to the interface. Hence, its zero level set determines the interface position. In order to track the interface movement, the following transport equation in primitive variables can be used

$$\frac{\partial \Phi}{\partial t} + \mathbf{v}\nabla\Phi = 0. \tag{12}$$

The level set function is advected by the fluid velocity $\mathbf{v}$. In our case, interface and fluid velocity are equal to each other as we do not take into account phase transition. To treat the level set function in a conservative manner, (12) is modified in the following way

$$\frac{\partial \Phi}{\partial t} + \nabla \cdot (\mathbf{v}\Phi) = \Phi\nabla \cdot (\mathbf{v}). \tag{13}$$

It is obvious that a new term appears on the right-hand side of the equation that has to be included as a source term.

3 The pressure-based Multiple Pressure Variables (MPV) method

The MPV scheme is a pressure-based method for the simulation of the compressible and the incompressible Euler equations. We directly use the Euler equations (1)-(3) in conservative formulation, according to [3]. To avoid the singularity in (10) for the incompressible limit $M = 0$, caused by the term $1/M^2 \nabla p$, the MPV scheme splits the pressure into multiple pressure variables, according to [2, 9]

$$p(x,t) = p^{(0)}(t) + M^2 p^{(2)}(x,t). \tag{14}$$

The leading order pressure term $p^{(0)}$ satisfies the EOS in the limit case $M = 0$ and it is therefore called thermodynamic background pressure. The spatially and temporally variable pressure $p^{(2)}$ can be considered to be a hydrodynamic pressure as it guarantees the divergence-free condition for incompressible flows at $M = 0$. Due to the pressure splitting, the term $1/M^2 \nabla p$ in equation (10) remains bounded in the incompressible limit and simply reduces to $\nabla p^{(2)}$. This pressure decomposition takes into account the fact that the pressure plays different roles in compressible and incompressible flows. For compressible flows, the pressure couples the density and the internal energy via the EOS. This directly results in a thermodynamic meaning. In case of an incompressible flow, the pressure loses its connection to density and energy as there is no EOS for this kind of flow. The pressure is of purely hydrodynamic nature.

Based on the above pressure decomposition, the energy equation (11) is reformulated in terms of pressure. For this purpose, the stiffened gas EOS (6) and the pressure decomposition (14) are inserted into the non-dimensional Euler equations (9)-(11) that result in the following system

$$\begin{pmatrix} \rho \\ \rho\mathbf{v} \\ p + \gamma p_\infty + (\gamma - 1)M^2 e_k \end{pmatrix}_t + \nabla \cdot \begin{pmatrix} \rho\mathbf{v} \\ (\rho\mathbf{v}) \circ \mathbf{v} + p^{(2)}\mathbf{I} \\ ((\gamma - 1)M^2 e_k + \gamma(p + p_\infty))\mathbf{v} \end{pmatrix} = \begin{pmatrix} 0 \\ 0 \\ 0 \end{pmatrix}. \tag{15}$$

Here, $\mathbf{I}$ designates the unity matrix. The most obvious change is apparent in the energy equation that is now expressed in a pressure formulation. Due to this reformulation, the MPV method uses the pressure as primary variable instead of the energy while the Euler equations are still in conservative formulation. As a next step the discretization of the above equations is discussed.

3.1 Time Discretization

Combining compressible and incompressible flows, the MPV approach builds upon a semi-implicit time discretization. This includes an explicit discretization of the convection terms while all terms linked to the speed of sound are discretized implicitly

$$\begin{pmatrix} \rho \\ \rho\mathbf{v} \\ p + \gamma p_\infty + (\gamma - 1)M^2 e_k \end{pmatrix}_t + \nabla \cdot \begin{pmatrix} \rho\mathbf{v} \\ (\rho\mathbf{v}) \circ \mathbf{v} \\ (\gamma - 1)M^2 e_k\mathbf{v} \end{pmatrix}^{ex} + \nabla \cdot \begin{pmatrix} 0 \\ p^{(2)}\mathbf{I} \\ \gamma(p + p_\infty)\mathbf{v} \end{pmatrix}^{im} = \begin{pmatrix} 0 \\ 0 \\ 0 \end{pmatrix}. \tag{16}$$

The superscripts ex and im designate the explicit and implicit time discretization of the respective terms. This procedure takes care of the physical and mathematical background. While the compressible Euler equations build a system of hyperbolic equations, the incompressible limit is described by a hyperbolic-elliptic system. Hence, pressure waves are traveling at infinite speed, the role of pressure in the Euler equations changes and requires an implicit treatment of the pressure terms. The semi-implicit discretization (16) clearly indicates that the density is treated independently in a fully explicit manner while momentum and energy equation contain explicit as well as implicit parts.

As it is common for incompressible projection methods, the MPV scheme finally is based on the solution of a Poisson equation derived by introducing the following predictor-corrector relations for pressure and velocity:

$$p^{(2)n+1} = p^{(2)*} + \delta p^{(2)}, \tag{17}$$

$$\mathbf{v}^{n+1} = \mathbf{v}^* + \delta \mathbf{v}. \tag{18}$$

The δ designates the corrector value for the corresponding predictor that is marked by the superscript $*$ and the superscript $n+1$ stands for the new time level.

In the following, the equations are discretized in time such that a semi-discrete formulation is obtained (still continuous in space but discrete in time). This approach is known as the method of lines where a partial differential equation (PDE) is transformed into an ordinary differential equation (ODE) by the choice of a spatial discretization. Afterwards, the resulting ODE can then be solved by an appropriate time discretization scheme. In general, the ODE that results from the semi-implicit MPV approach can be written as follows

$$\frac{d\mathbf{U}}{dt} = \mathbf{f}(\mathbf{U}^n) + \mathbf{g}(\mathbf{U}^{n+1}), \tag{19}$$

where $\mathbf{U}$ designates the vector of the discretized conservative variables of the Euler equations and Δt stands for the discrete time step. The operator $\mathbf{f}(\mathbf{U^n})$ represents the explicitly discretized, non-stiff convective terms while the stiff terms are discretized implicitly and grouped together in the operator $\mathbf{g}(\mathbf{U^{n+1}})$.

At present, we use two different time discretizations that are of first and second order accuracy. The first order scheme uses the simple explicit and implicit Euler method that can be expressed as follows

$$\mathbf{U}^{n+1} = \mathbf{U}^n + \Delta t \left[\mathbf{f}(\mathbf{U}^n) + \mathbf{g}(\mathbf{U}^{n+1}) \right]. \tag{20}$$

To achieve a second order temporal discretization method, we use a combination of Runge-Kutta for the explicit part and Crank-Nicolson for the implicit terms of the MPV approach (RK2CN). This approach necessitates the introduction of a half time level

$$\mathbf{U}^{n+1/2} = \mathbf{U}^n + \frac{\Delta t}{2} \left[\mathbf{f}(\mathbf{U}^n) + \mathbf{g}(\mathbf{U}^{n+1/2}) \right], \tag{21}$$

$$\mathbf{U}^{n+1} = \mathbf{U}^n + \Delta t \mathbf{f}(\mathbf{U}^{n+1/2}) + \frac{\Delta t}{2} \left[\mathbf{g}(\mathbf{U}^n) + \mathbf{g}(\mathbf{U}^{n+1}) \right]. \tag{22}$$

For the sake of simplicity, the following description of the numerical scheme is limited to the first order time discretization. Starting with the pressure $p^{(2)n}$ at the old time level as a guess for the predictor $p^{(2)*}$, the velocity $\mathbf{v}^*$ follows directly from the momentum equation. Based on the Euler explicit and implicit scheme, we obtain a relation between the two correctors $\delta \mathbf{v}$ and $\delta p^{(2)}$ from the momentum equations

$$\delta \mathbf{v} = -\Delta t \frac{\nabla \delta p^{(2)}}{\rho^{n+1}}. \tag{23}$$

The two correctors $\delta p^{(2)}$ for pressure and $\delta \mathbf{v}$ for velocity are introduced into the energy equation of system (16) together with (23). This results in a Poisson equation for the pressure corrector $\delta p^{(2)}$

$$M^2 \delta p^{(2)} - \Delta t^2 \nabla \cdot \left[\frac{\gamma(p^e + p_\infty)}{\rho^{n+1}} \nabla \delta p^{(2)} \right] = M^2 [p^{(2)n} - p^{(2)*}] - dp^{(0)n} - \Delta t \nabla \cdot (\gamma(p^e + p_\infty) \mathbf{v}^*) - (\gamma-1)M^2 \delta k^*, \tag{24}$$

where p^e is a tentative value for the pressure at the new time level and $dp^{(0)n}$ describes the effects of outer compression originating from the domain boundaries. The term δk^* represents the contribution of the kinetic energy e_k

$$\delta k^* = e_k^* - e_k^n + \Delta t \nabla \cdot (e_k \mathbf{v}). \tag{25}$$

The kinetic energy e_k^* is an approximation to the energy at the new time level, evaluated by the use of the explicitly determined density ρ^{n+1} and the predictor velocity $\mathbf{v}^*$. Due to the use of p^e and e_k^* the Poisson equation is linearized and solved in an iterative way until convergence of $\delta p^{(2)}$ is reached. Then, pressure and velocity can be updated in the whole flow domain. A more detailed description of the numerical method can be found in [3].

3.2 Space Discretization

The spatial discretization is carried out on a Cartesian, staggered grid in three space dimensions, according to [10]. For the purpose of explanation, such a mesh is depicted in Fig. 1 for the two-dimensional case. It
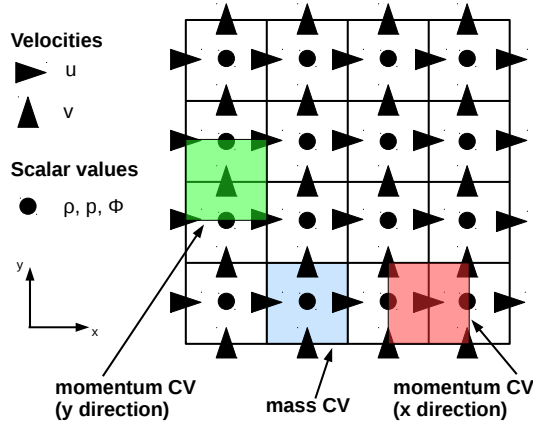

Figure 1: Staggered grid arrangement: overview over variables and different control volumes (CV).

is obvious, that there are different control volumes (CV) for mass and momentum. While all scalar values like density, pressure and the level set function are located at the cell center of the mass CV, the velocity components are stored at the center of the momentum CV that coincides with the center of the mass CV cell faces. The same principle is applied in three dimensions. The convective fluxes for the first order spatial discretization are evaluated in a simple upwind manner. For the second order version, a linear reconstruction is performed based on the MUSCL approach [11].

3.3 Interface Tracking

The DNS of compressible two-phase flows is a rather challenging task as the two fluids often differ significantly in their material properties as well as in their thermodynamic behavior expressed by the EOS. For this reason,
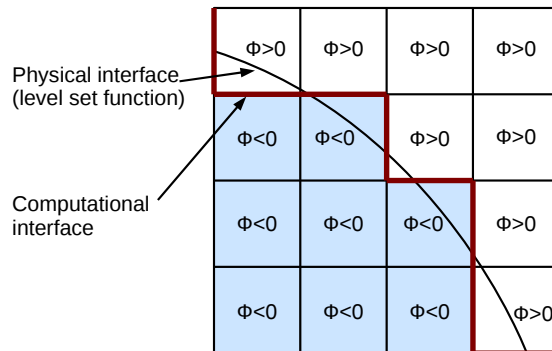

Figure 2: Physical and computational interface.

it is crucial to accurately know and track the interface location at each time step. With the introduction of the level set function Φ and the corresponding transport equation (12), we are able to describe and evolve the material interface in the course of the computation. The level set Φ is initialized as a signed distance function, such that its zero level set coincides with the interface location. Hence, we are able to easily assign the different fluids by the sign of the level set. While Φ has a positive sign in the gaseous phase, it is negative in the liquid phase.

Due to the use of the general stiffened gas EOS formulation (6) the MPV method offers the possibility

6

to treat two different fluids distinguished by their values of the constants γ and p_∞. For the multiphase computation, both constants are allowed to vary from one grid cell to another such that each cell (i, j, k) is assigned to specific values $\gamma_{(i,j,k)}$ and $p_{\infty,(i,j,k)}$. At each time step, a loop over all grid cells is performed and based on the level set variable the corresponding values $\gamma_{(i,j,k)}$ and $p_{\infty,(i,j,k)}$ are set. This treatment shifts the physical interface to the cell faces, creating a computational interface that is of staircase shape, as it can be seen in Fig. 2. Once $\gamma_{(i,j,k)}$ and $p_{\infty,(i,j,k)}$ are assigned, the usual MPV solution procedure of the Poisson equation can be applied, taking into account the spatially variable constants

$$M^2 \delta p^{(2)} - \Delta t^2 \nabla \cdot \left[\frac{\gamma_{(i,j,k)}(p^e + p_{\infty,(i,j,k)})}{\rho^{n+1}} \nabla \delta p^{(2)} \right] =$$

$$M^2[p^{(2)n} - p^{(2)*}] - dp^{(0)n} - \Delta t \nabla \cdot (\gamma_{(i,j,k)}(p^e + p_{\infty,(i,j,k)})\mathbf{v}^*) - (\gamma_{(i,j,k)} - 1)M^2 \delta k^*. \qquad (26)$$

The material interface represents a discontinuity in the EOS that may lead to spurious pressure and velocity oscillations at this location, especially when density-based flow solvers in conservative formulation are used without any special interface treatment [1]. Our approach based on the conservative MPV method does not need any special interface treatment to prevent oscillations. This can be easily explained for the transport of a density contact discontinuity with the first order spatial discretization. In this case, velocity and pressure are constant in the whole flow domain and only density is jumping across the contact discontinuity. In general, pressure is the primary variable of the MPV scheme and velocity is directly linked to it (cf. equation (23)). At each time step, pressure and velocity are updated by solving the Poisson equation (24). It can easily be shown that the right-hand side of (24) is always equal to zero for constant pressure and velocity. Therefore, the pressure corrector is also equal to zero $\delta p^{(2)} = 0$ everywhere so that pressure and velocity remain unchanged and the scheme is oscillation-free in the vicinity of the interface.

3.4 Interface tracking using a discontinuous Galerkin approach

To improve the interface resolution, a high-order DG scheme can be applied to the interface tracking (13). Using a high order scheme, the surface can be described more precisely. This is crucial for the evaluation of the surface normals and curvature that are needed in order to include surface tension and other physical phenomena that are directly linked to the topology of the interface. The level set equation can be treated independently from the flow solver. For this reason it is easily possible to discretize (13) with a numerical scheme that is different from the flow solver. We use a high-order discontinuous Galerkin spectral element method [5] that is also employed for the interface tracking in [6]. For the coupling of the finite volume flow

(a) Coupling cycle: MPV flow solver and DG level set solver.

(b) Reconstruction of the velocity distribution inside a DG cell. For each small cell the integral over the polynomial of the bigger cell is equal to its integral mean value.
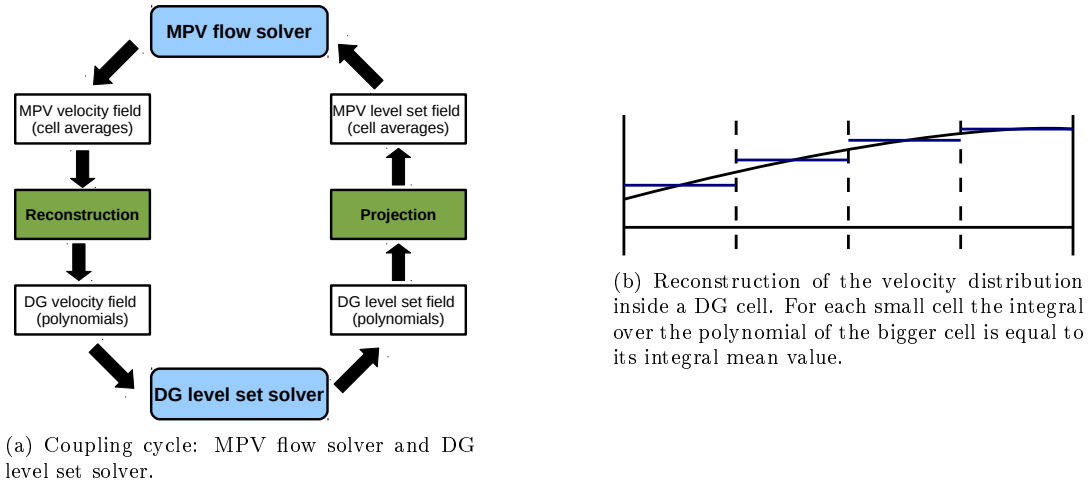
Figure 3: Coupling of the MPV scheme with the DG solver.

solver with the DG approach, appropriate data interfaces have to be defined. This concerns the fluid velocity and the level set variable itself. The DG solver advects the level set function on the basis of the fluid velocity

field, calculated by the flow solver. Once the level set field has been updated by the DG approach, it is passed back to the flow solver, together with the surface normals and curvature. The following reconstruction and projection steps have to be performed to provide the two solvers with appropriate data. On the one hand, for the DG scheme it is necessary to reconstruct velocity polynomials from the finite volume velocity distribution. On the other hand, the level set polynomial has to be projected to finite volume cell averages that can be used by the MPV flow solver. The whole coupling cycle is illustrated in Fig. 3(a).

The reconstruction step is depicted in Fig. 3(b) in 1D. The desired polynomial inside each DG cell is obtained by grouping several finite volume cells together to a bigger DG cell. The number of finite volume cells that are summarized to a DG cell depends directly on the polynomial degree N of the DG approach. In case of the 1D sketch, $N = 3$ is chosen and four finite volume cells build a DG cell in which a polynomial is reconstructed from the cell averages of the smaller cells. For the reconstruction, we demand that the integral over the DG polynomial in each small cell is equal to the corresponding cell average of the small finite volume cell. To project the updated level set field on the finite volume cells, the inverse procedure is applied.

4 Results

In the following, two numerical test cases are presented. Both of them are shock-droplet interactions and we use the following setup, unless otherwise stated. The ideal gas EOS with $\gamma = 1.4$ is used for the surrounding gas phase and the stiffened gas EOS with $p_\infty = 3309$ for the liquid phase inside the droplet. The computations are carried out with the second order RK2CN MPV method and we use 64 grid cells in each of the three spatial directions.

4.1 Shock-droplet interaction: single droplet

The first test case describes the impact of an initially planar shock wave on a spherical droplet. The initial conditions of the test case are specified in Fig. 4 that also shows the pressure distribution on a slice through the center of the droplet at the instant $t = 4.25 \cdot 10^{-3}$. A more detailed analysis of the pressure field can be
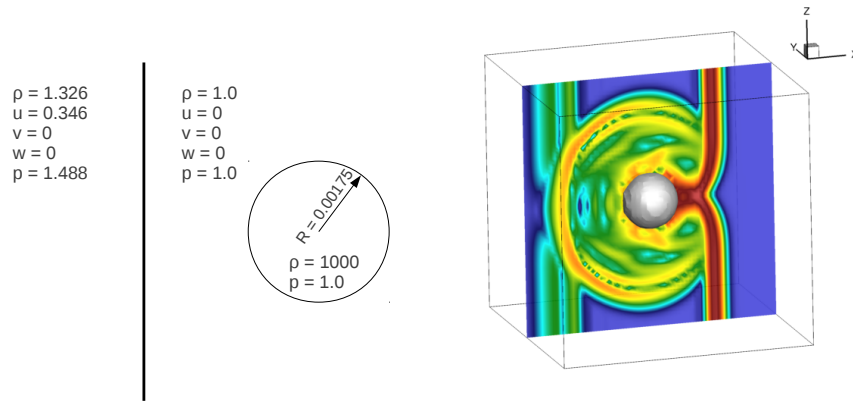

Figure 4: Sketch of the setup for the 3D shock-droplet interaction test case (left) and a slice through the droplet center at $t = 4.25 \cdot 10^{-3}$ showing the pressure gradient $\log(|\nabla p| + 1)$ (right).

carried out by having a closer look at the pressure and pressure gradient distributions at different instants that are given in Fig. 5. Plotting the gradient of the pressure, the wave structures can be resolved in more detail. When the shock wave is impinging on the droplet surface, the shock is reflected as well as transmitted into the droplet. While the reflected wave forms a bow shock due to the spherical geometry of the droplet, the transmitted wave is traveling through the droplet. Because of the higher speed of sound inside the droplet, the shock wave obviously is moving faster inside than outside. This is evident from the plot at $t_1 = 1.5 \cdot 10^{-3}$ in Fig. 5. The pressure distribution inside the droplet is no longer uniform indicating that the shock has already traveled through the complete droplet. Moreover, the shock is reflected at the rear part

as an expansion that is moving back to the front. During the following time steps, the waves are reflected several times inside the droplet. At $t_2 = 4.25 \cdot 10^{-3}$, the shock wave has made its way around the droplet and the waves are interacting at the rear part, forming a curved shock front. Looking at the plots of pressure and pressure gradient, both are indicating a perfectly symmetric distribution.
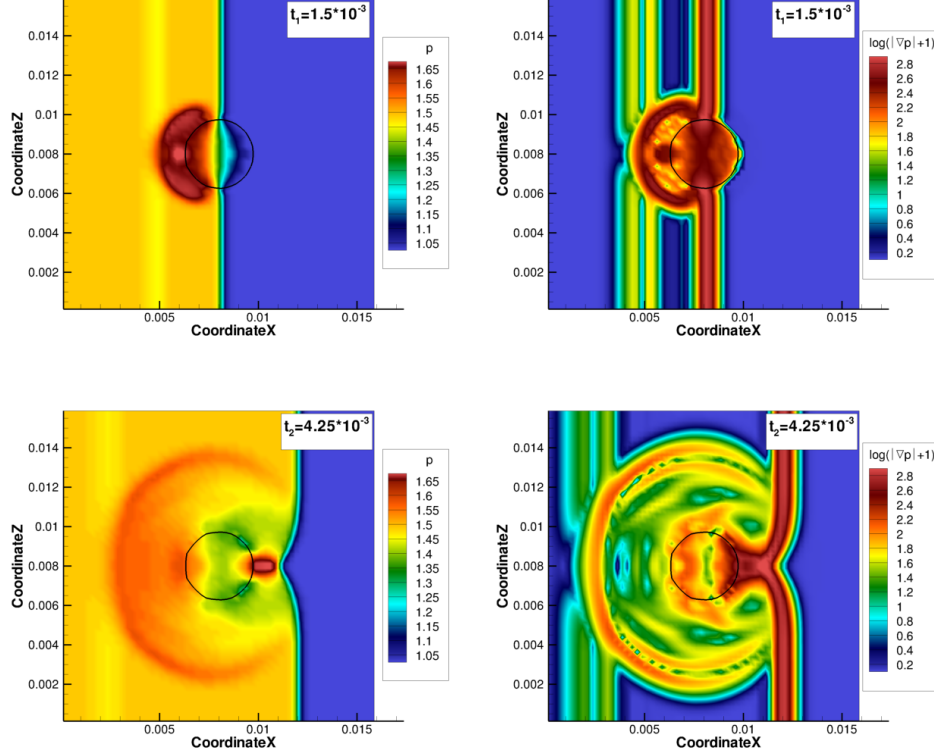

Figure 5: Pressure p and pressure gradient $\log(|\nabla p|+1)$ at $t_1 = 1.5 \cdot 10^{-3}$ (top) and $t_2 = 4.25 \cdot 10^{-3}$ (bottom). 3D shock-droplet interaction test case, slices through the droplet center.

The MPV method with the above presented interface treatment is not suffering from any pressure or velocity oscillations near the interface. This is illustrated by Fig. 6. The contour lines of pressure show a smooth transition between the two phases. Additionally, the velocity vectors are not indicating any oscillations. Hence, the pressure-based MPV method proves to give oscillation-free results for the 3D simulation of compressible two-phase flows.

4.2 Shock-droplet interaction: two droplets

For this test case, a second spherical droplet is introduced. This generates additional wave reflections and interactions that finally result in a more complex wave pattern. The initial setup is presented in Fig. 7 as well as the pressure gradient distribution on a slice through the droplet centers at the time $t = 5 \cdot 10^{-3}$. Similar to the single droplet case, Fig. 8 illustrates the pressure as well as the pressure gradient distribution at the instant $t = 5 \cdot 10^{-3}$. It can be seen, that we have a non-symmetric pressure distribution inside the bigger droplet. This is due to the presence of the smaller droplet. The right moving initial shock wave finally impinges on the surface of the smaller droplet where it is reflected. The reflected wave has a curved shape, it travels back towards the bigger droplet and hits its surface in the rear part. This impact influences the wave pattern inside the big droplet.

In Fig. 9 we compare a 3D simulation to a two-dimensional one at $t = 1.6 \cdot 10^{-3}$. There are two remarkable points. First of all, the wave patterns inside the droplets look different. This is due to 3D effects, caused by the spherical shape of the 3D droplet that causes differences in the wave reflections in comparison to the
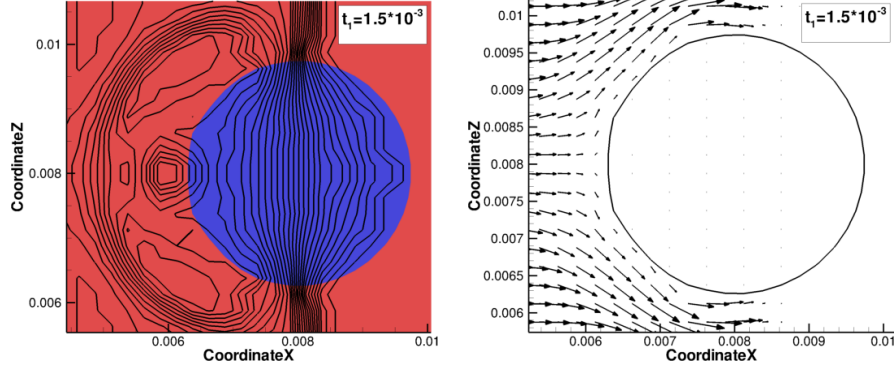
Figure 6: Contour lines of pressure (left) and velocity field with vectors at each grid node (right) for the 3D shock-droplet interaction test case. Slice through the droplet center at $t = 1.5 \cdot 10^{-3}$.
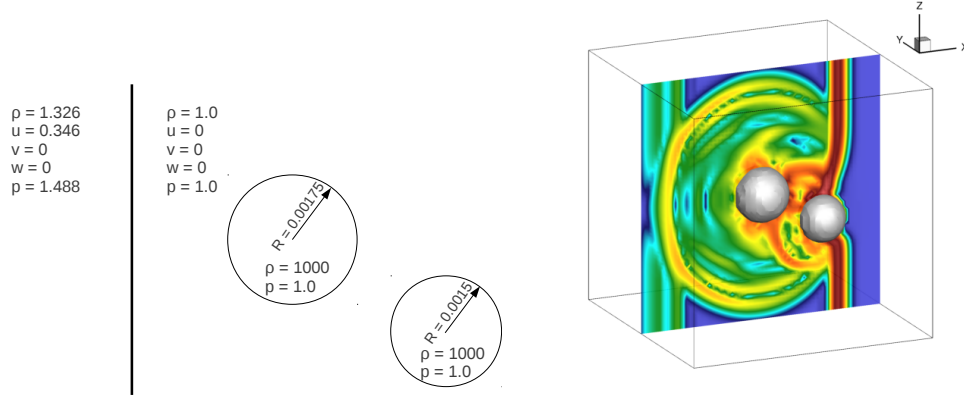

Figure 7: Sketch of the setup for the 3D shock-droplet interaction test case including two spherical droplets (left) and a slice through the droplet centers at $t = 5 \cdot 10^{-3}$ showing the pressure gradient $\log(|\nabla p| + 1)$ (right).

2D case. Moreover, behind the bigger droplet, a very weak shock wave is visible in both cases. This wave is transmitted through the droplet. It is clearly more pronounced in the 2D case than in the 3D calculation.

4.3   Shock-droplet interaction: single droplet with level set DG approach

The level set DG approach of section 3.4 is applied to the above introduced shock-droplet interaction with a single droplet. The numerical scheme is used with a spatial resolution of 60^3 finite volume cells and the DG scheme uses a polynomial of the degree $N = 3$. This choice directly results in 15^3 grid cells for the DG scheme. Figure 10 illustrates the distributions of pressure and pressure gradient inside the droplet at the time $t_1 = 7.5 \cdot 10^{-4}$. The propagation of the shock wave is clearly visible and both plots are consistent with the previous results. Moreover, the cut through the droplet shows a perfectly circular interface. However, if we continue the computation the results look different from those of Fig. 5. The interface gets crinkled and this change in topology causes considerable changes in the pressure distribution. Hence, later instants in time are not accessible by our scheme yet and we are currently investigating the unphysical topology changes of the interface. We suppose that the problem might be linked to the velocity reconstruction. Oscillations of the velocity polynomials may cause the spurious interface deformation.
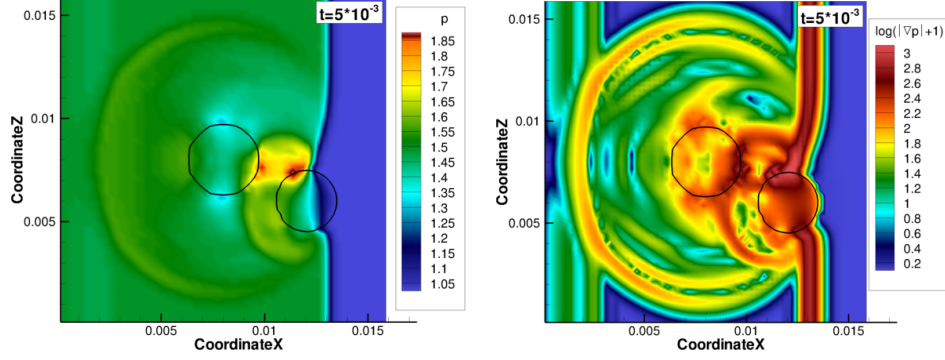
Figure 8: Pressure p and pressure gradient $\log(|\nabla p| + 1)$ at $t = 5 \cdot 10^{-3}$. Slices through the droplet centers.
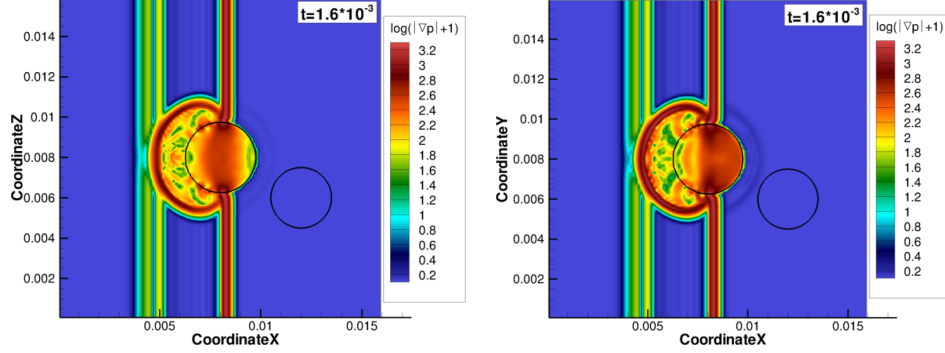

Figure 9: Pressure gradient $\log(|\nabla p| + 1)$ at $t = 1.6 \cdot 10^{-3}$ for the 3D (128^3 grid cells, slice through the droplet center; left) and the 2D (128^2 grid cells; right) calculation of the shock-droplet interaction with two droplets.
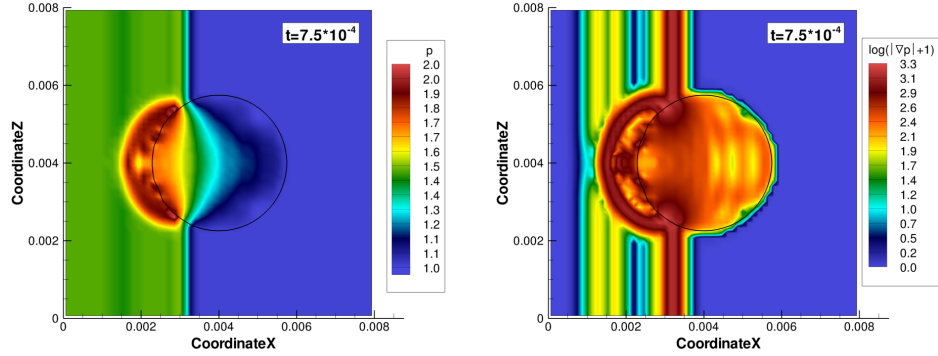

Figure 10: Pressure and pressure gradient $\log(|\nabla p| + 1)$ at $t = 7.5 \cdot 10^{-4}$ on a slice through the droplet center for the coupled MPV level set DG approach. 3D calculation of the shock-droplet interaction (60^3 finite volume grid cells, 15^3 DG grid cells with polynomial degree $N = 3$).

5   Conclusions

In this paper a pressure-based numerical scheme for the simulation of 3D compressible two-phase flows is presented. The algorithm is based on an asymptotic pressure expansion. It can be used to extend originally incompressible multiphase methods to the compressible flow regime as it formally allows the simulation of incompressible as well as compressible flows. Unlike many other approaches for compressible two-phase flows that encounter spurious oscillations at the material interface, a cumbersome special interface treatment can be avoided. The physical interface is described by the zero level set function and it is shifted to the cell boundaries for the computations. Two different approaches for the transport of the level set variable are shown, a standard finite volume discretization and a high-order DG approach. Two multidimensional test cases are shown and the MPV method proves to resolve complex wave patterns including several wave reflections inside and outside of liquid droplets. The DG approach for the interface tracking still suffers from spurious wiggles that develop in the course of the computation. Their elimination is in the scope of the future work, finally resulting in an enhanced interface resolution that is supposed to be beneficial for the simulation of interfacial phenomena, like surface tension. Surface tension is strongly dependent on the curvature and the interface needs to be resolved accurately in order to get appropriate estimates for the surface normals and curvature from the level set function. The polynomial representation of the level set by the DG scheme allows to easily and accurately evaluate the desired values. Furthermore, we plan to include viscous effects and to extend the numerical scheme to the compressible Navier-Stokes equations.

6   Acknowledgements

References

[1] R. Abgrall and S. Karni. Computations of compressible multifluids. *J. Comput. Phys.*, 169:594–623, 2001.

[2] C.-D. Munz, S. Roller, R. Klein and K.J. Geratz. The extension of incompressible flow solvers to the weakly compressible regime. *Comput. Fluids*, 32(2):173–196, 2003.

[3] J.H. Park and C.-D. Munz. Multiple pressure variables methods for fluid flow at all Mach numbers. *Int. J. Numer. Meth. Fl.*, 49:905–931, 2005.

[4] M. Boger, F. Jaegle and C.-D. Munz. A Pressure-Based Method for the Direct Numerical Simulation of Compressible Two-Phase Flows. Proc. 24th European Conference on Liquid Atomization and Spray Systems, Estoril, Portugal, 2011.

[5] D. A. Kopriva. *Spectral Element Methods*. Springer, 2009.

[6] S. Fechter, F. Jaegle, M. Boger, C. Zeiler and C.-D. Munz. A discontinuous Galerkin based multiscale method for compressible multiphase flow. Proc. 7th International Conference on Computational Fluid Dynamics, Big Island, Hawaii, 2012.

[7] R. Saurel and R. Abgrall. A simple method for compressible multifluid flows. *SIAM J. Sci. Comp.*, 21(3):1115–1145, 1999.

[8] S. Osher and J.A. Sethian. Fronts propagating with curvature-dependent speed: Algorithms based on Hamilton-Jacobi formulations. *J. Comput. Phys.*, 79(1):12–49, 1988.

[9] S. Klainerman and A. Majda. Compressible and incompressible fluids. *Commun. Pur. Appl. Math.*, 35:629–653, 1982.

[10] A.T. Harlow and J.E. Welch. Numerical calculation of time-dependent viscous incompressible flow of fluid with a free surface. *Phys. Fluids*, 8:2182–2189, 1965.

[11] B. van Leer. Towards the ultimate conservative difference scheme. V. A second-order sequel to Godunov's method. *J. Comput. Phys.*, 32:101–136, 1979.